PNAS RESEARCH ARTICLE | CHEMISTRY
BIOPHYSICS AND COMPUTATIONAL BIOLOGY

An uncharacteristically low-potential flavin governs the energy landscape of electron bifurcation

Courtney E. Wise[a], Anastasia E. Ledinina[a], David W. Mulder[a], Katherine J. Chou[a], John W. Peters[b], Paul W. King[a], and Carolyn E. Lubner[a,1]

Edited by Peter Rossky, Rice University, Houston, TX; received September 28, 2021; accepted January 24, 2022

Electron bifurcation, an energy-conserving process utilized extensively throughout all domains of life, represents an elegant means of generating high-energy products from substrates with less reducing potential. The coordinated coupling of exergonic and endergonic reactions has been shown to operate over an electrochemical potential of ∼1.3 V through the activity of a unique flavin cofactor in the enzyme NADH-dependent ferredoxin-NADP$^+$ oxidoreductase I. The inferred energy landscape has features unprecedented in biochemistry and presents novel energetic challenges, the most intriguing being a large thermodynamically uphill step for the first electron transfer of the bifurcation reaction. However, ambiguities in the energy landscape at the bifurcating site deriving from overlapping flavin spectral signatures have impeded a comprehensive understanding of the specific mechanistic contributions afforded by thermodynamic and kinetic factors. Here, we elucidate an uncharacteristically low two-electron potential of the bifurcating flavin, resolving the energetic challenge of the first bifurcation event.

biophysics | electron bifurcation | energy conservation | flavoenzyme | thermodynamics

Enzymes drive energetically challenging chemical reactions with high efficiency and fidelity by employing innovative solutions for overcoming thermodynamic and kinetic barriers. This is particularly true for electron bifurcating enzymes, which separate a pair of electrons at a single cofactor and direct each along spatially and thermodynamically distinct pathways that conclude with delivery of the individual electrons to different products (1–8). Bifurcating systems utilize the free energy generated from an initial exergonic oxidation-reduction reaction along a high-potential catalytic branch to drive a coupled endergonic one across a low-potential pathway (9, 10). This results in an overall spontaneous process which conserves energy and produces more potent reducing equivalents than the substrate initiating catalysis (11–13). Bifurcation can be especially critical for optimal efficiency in anaerobic metabolism, where certain reactions necessitate reducing equivalents from donors with potentials more negative than the pyridine nucleotide-based energetic currency of the cell (14–17).

In the flavin-based electron bifurcating (FBEB) enzyme NADH-dependent ferredoxin:NADP$^+$-oxidoreductase (NfnSL), a central FAD cofactor facilitates the reduction of NAD$^+$ and ferredoxin (Fd) (Fig. 1) (4, 18). Briefly, NADPH binds at the bifurcating flavin site, L-FAD, donating a hydride to form the fully reduced flavin hydroquinone (HQ) species. Electrons are then bifurcated, with the first being transferred to the high-potential pathway in the small subunit, NfnS. This electron transfer (ET) event generates a high-energy, short-lived anionic semiquinone (ASQ) at L-FAD and results in rapid ET to the low-potential pathway of the large subunit, NfnL (4). A second round of bifurcation occurs to produce 1 NADH and 2 reduced Fd (Eq. **1**).

$$2\ \mathrm{NADPH} + \mathrm{NAD}^+ + 2\ \mathrm{Fd}_{\mathrm{ox}} \rightleftharpoons 2\ \mathrm{NADP}^+ + \mathrm{NADH} + 2\ \mathrm{Fd}_{\mathrm{red}} + \mathrm{H}^+. \quad [1]$$

One striking feature of NfnSL is the energetic landscape of the bifurcation reaction, which has been reported to span 1.27 V of electrochemical potential energy (4). This derives from the inverted reduction potentials of the bifurcating flavin, thought to be a key requirement for FBEB (4, 9, 19, 20), whereby the reduction of oxidized (Ox) flavin to the ASQ state occurs at a potential more negative than the reduction of ASQ to HQ (21). Physically, inverted potentials manifest as a destabilized, one-electron reduced flavin semiquinone species, rendering them challenging to observe and characterize experimentally. Despite this, the half-life of the ASQ intermediate was measured to be 10 ps for NfnSL (4, 9). Based in part on this information, the one-electron reduction potential for the Ox-to-ASQ couple ($E_{\mathrm{m,Ox/ASQ}}$) was determined to be −911 mV versus SHE (see *SI Appendix* for more details), demonstrating how NfnSL capitalizes on the inverted potentials of L-FAD to drive reduction of the high-energy Fd substrate (4, 22). Although this result was obtained from methodology specifically

Significance

Nature has long been an inspiration for materials design, as it exemplifies exquisite control of both matter and energy. Electron bifurcation, a mechanism employed in biological systems to drive thermodynamically unfavorable and energetically challenging chemical reactions, is one such example. A key feature of bifurcating enzymes is the ability of a single redox cofactor to distribute a pair of electrons across two spatially separated electron transfer pathways. Here, we report on the empirical determination of both the one-electron potential and two-electron potential of the bifurcating flavin cofactor in the NADH-dependent ferredoxin-NADP$^+$ oxidoreductase I (NfnSL) enzyme. Insights arising from the defined energy landscape of this bifurcation site may underlie the design of synthetic catalysts capable of generating high-energy intermediates.

Author affiliations: [a]Biosciences Center, National Renewable Energy Laboratory, Golden, CO 80401; and [b]Institute of Biological Chemistry, Washington State University, Pullman, WA 99163

Author contributions: C.E.W. and C.E.L. designed research; C.E.W., A.E.L., D.W.M., and C.E.L. performed research; K.J.C. contributed new reagents/analytic tools; C.E.W., D.W.M., and C.E.L. analyzed data; and C.E.W., D.W.M., J.W.P., P.W.K., and C.E.L. wrote the paper.

The authors declare no competing interest.

This article is a PNAS Direct Submission.

[1]To whom correspondence may be addressed. Email: cara.lubner@nrel.gov.

This article contains supporting information online at http://www.pnas.org/lookup/suppl/doi:10.1073/pnas.2117882119/-/DCSupplemental.

Published March 15, 2022.

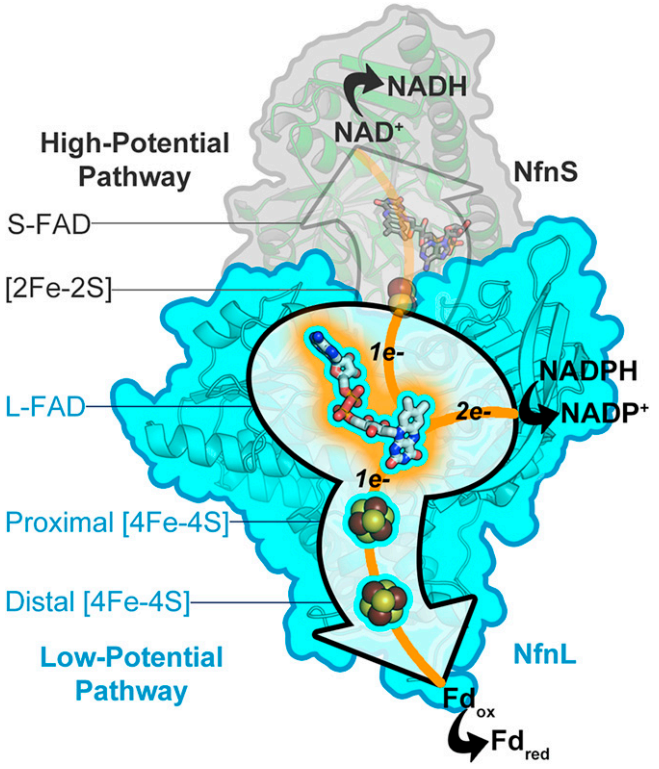

Fig. 1. NfnSL from *Pyrococcus furiosus* (*Pf*) (PDB 5JFC) (4) is comprised of a large subunit (NfnL, blue) and a small subunit (NfnS, gray). Following oxidation of NADPH, the bifurcating flavin, L-FAD (center), performs two one-electron transfers, first to the site-differentiated [2Fe-2S] of NfnS, then to the site-differentiated proximal [4Fe-4S] cluster of NfnL. The [2Fe-2S] is oxidized by S-FAD, which catalyzes the reduction of NAD^+ to NADH following two rounds of bifurcation. The proximal NfnL cluster reduces the distal [4Fe-4S], which subsequently reduces one equivalent of ferredoxin (Fd) for each NADPH oxidized.

assessing L-FAD, the presence of an additional flavin, S-FAD, obscured unambiguous assignment of the L-FAD two-electron couple ($E_{m,Ox/HQ}$). The previously obtained $E_{m,Ox/HQ}$ of −276 mV (4), thought to represent the average potential of the two flavins, has had profound implications for defining the energy landscape of NfnSL with the most significant being the rather large uphill initial electron bifurcation step (+359 mV L-FAD HQ donor to +80 mV [2Fe-2S] acceptor) (23). It is imperative to achieve an accurate description of the reduction potentials of L-FAD in order to elucidate the determinants that control and initiate electron bifurcation. Given the scarcity of information on bifurcating flavins, along with the fact that values are often inferred from related systems (24–27) and the impact that this has on further studies, it is especially prudent.

Here, we have utilized a recombinant expression system for production of the NfnSL holoenzyme, which is comprised of a small (NfnS) and large (NfnL) subunit, and the isolated NfnL subunit to establish an accurate biophysical description of the bifurcating flavin. Data regarding the kinetics of the L-FAD ASQ intermediate from transient absorption (TA) spectroscopy analyses were consistent with previous observations in NfnSL, indicating the Ox/ASQ couple of the bifurcating flavin is unchanged in the absence of NfnS. Spectroelectrochemical (SEC) studies revealed a two-electron reduction potential for L-FAD that is more negative than previously thought and square wave voltammetry (SWV) allowed for elucidation of the L-FAD one-electron ASQ/HQ couple alongside improved resolution of the NfnL [4Fe-4S] cluster potentials. The results of this study facilitate greater insight into the energy transformation and coupling mechanisms employed in flavin-based electron bifurcating systems.

Results and Discussion

Recombinant expression of the NfnSL and NfnL constructs resulted in high yields of purified protein and reconstitution of flavin and iron-sulfur (Fe/S) content allowed for cofactor-replete holoenzymes that exhibited dye-based steady-state kinetics activity with NADPH (*SI Appendix*, Fig. S1). Details on the plasmid DNA constructs, expression, purification, reconstitution, and cofactor quantification can be found in the *SI Appendix*. The unsurprising greater than fivefold decrease in activity with NfnL relative to NfnSL likely derives from the disruption to the reaction coordinate, because NfnL alone is unable to bifurcate electrons. Electron paramagnetic resonance (*SI Appendix*) analyses of NADPH- and dithionite-reduced NfnL were consistent with previous assessments but allowed for a more concrete assignment of the *g*-values for both [4Fe-4S] clusters due to the lack of signal overlap with cofactors in NfnS (*SI Appendix*, Fig. S2).

Spectroelectrochemical studies of NfnL revealed an $E_{m,Ox/HQ}$ for the bifurcating flavin of −436 ± 8 mV (Fig. 2). This value, which is considerably lower than previously reported, significantly impacts the extent of the energy gap utilized by NfnSL along with all three of the ET reactions that L-FAD participates in. Specifically, insights into the mechanisms employed within the high-potential branch and those governing the initiation of bifurcated ET have emerged from this result and are discussed in detail below. Additionally, this data suggests that the S-FAD redox potential values may require further refinement. Transient absorption spectroscopy (*SI Appendix*) verified that the L-FAD of isolated NfnL retained its ability to form an ASQ intermediate with a half-life of 10.8 ± 0.7 ps, which is comparable to previous measurements with NfnSL (10.2 ± 0.2 ps) (4) (*SI Appendix*, Fig. S3). This indicates that the Ox/ASQ potential for this flavin is

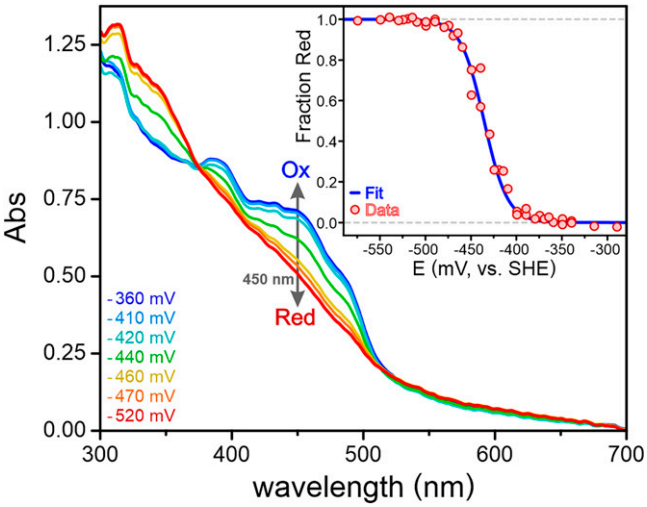

Fig. 2. Data (*Inset*) and representative spectra from spectroelectrochemical measurements showing the reversible, two-electron Ox/HQ couple of L-FAD at pH 8.8 and room temperature. Flavin reduction was monitored using the decrease (Ox-to-Red) or increase (Red-to-Ox) in absorbance at 450 nm (gray arrow), where the Fe/S cofactors of NfnL have little spectral interference. The fraction of reduced L-FAD (*Inset*, red) was derived from the absorbance change at this wavelength and plotted as a function of the applied potential, then fit to a Nernst function (*Inset*, blue). The fitted data of replicate measurements resulted in a potential of −436 ± 8 mV and n = 2.0 ± 0.1 electrons.

not significantly altered by the absence of NfnS and remains exceptionally low.

A bifurcating site with such low potential presents salient implications for the interactions between NfnSL and NADP(H). While NADP(H) has a formal reduction potential at pH 7.0 of −320 mV (28, 29), the E° exhibits a pH dependence of 30.1 mV per pH unit (28). The implications are twofold; first, NADPH possesses a more negative potential (−374 mV) in our studies due to the higher pH of 8.8 employed here. Second, the half-cell reduction potential, E, for a compound is highly dependent on the ratio of its reduced and oxidized species according to the Nernst equation (30). Modulation of the NADPH:$NADP^+$ ratio has resulted in reported potentials ranging from −190 to −420 mV for different organisms and growth conditions (11, 29, 31–33). This ratio is generally stated to be ∼100:1 in cells (34), which would provide a sufficient thermodynamic driving force for reduction of L-FAD. Further, it is likely that reduction of L-FAD by NADPH occurs through a hydride transfer event, which would implicate more complexity than can be appropriately summarized by the thermodynamics of electron donor and acceptor potentials. Fluorescence spectroscopy experiments were performed that revealed a K_D of 3.0 ± 0.4 μM (*SI Appendix*, Fig. S4) for NfnL with NADP(H), indicating tight binding, with no appreciable difference in affinity for the oxidized versus reduced substrate. Such a tight interaction between NfnSL and the NADP(H) substrate acts to further aid in initiating catalysis with the low potential bifurcating site.

Protein-film square wave voltammetry (SWV), a sensitive pulsed technique capable of detecting species that accumulate only to trace levels (35), was used to assess the reduction potentials of the NfnL [4Fe-4S] clusters. Compared to previous electrochemistry with NfnSL, NfnL showed a more pronounced signal from the proximal cluster and a slightly more positive E_m value of −670 mV, while the distal cluster exhibited a peak with a sharper intensity distribution at −518 mV in the reducing direction that resembled contribution from an additional signal (likely a two-electron transition) (*SI Appendix*, Fig. S5). It was hypothesized that the altered distal cluster signal distribution and the ∼+50 mV change in proximal cluster E_m derived from significant peak overlap between the two [4Fe-4S] clusters and the L-FAD $E_{m,Ox/HQ}$. To assess this possibility, SWV analysis was performed on NfnL reconstituted only with iron and sulfur (FeS-NfnL, retaining 0.35 equivalents FAD). FeS-NfnL exhibited more homogeneity in Fe/S signal shape and intensity at −701 and −529 mV, assigned as the proximal and distal clusters respectively, which indicated that the deviations observed with NfnL primarily owed to overlapping signals of the three NfnL cofactors. This was supported by analysis of the SWV signals (*SI Appendix*, Table S1), which showed the flavin contribution in FeS-NfnL to be 36 ± 2% that of holo-NfnL.

An additional SWV signal at +40 ± 4 mV was observed for NfnL only in the oxidizing direction and was diminished in FeS-NfnL (Fig. 3). This was assigned to the L-FAD $E_{m,ASQ/HQ}$ (see *SI Appendix* for further explanation), in excellent agreement with the calculated value of +39 mV (*SI Appendix*, Table S2) from the measured L-FAD $E_{m,Ox/HQ}$ and $E_{m,Ox/ASQ}$ (Eq. **3**). This signal was also observed in NfnSL (*SI Appendix*, Fig. S6), indicating minimal influence on the L-FAD potentials from the absence of NfnS. No other signals were observed at higher potentials in oxidizing scans of NfnL (*SI Appendix*, Fig. S7). Significantly, the +40 mV L-FAD $E_{m,ASQ/HQ}$ renders the first bifurcated ET to the +80 mV [2Fe-2S] energetically favorable, whereas it was previously thought to be uphill with an

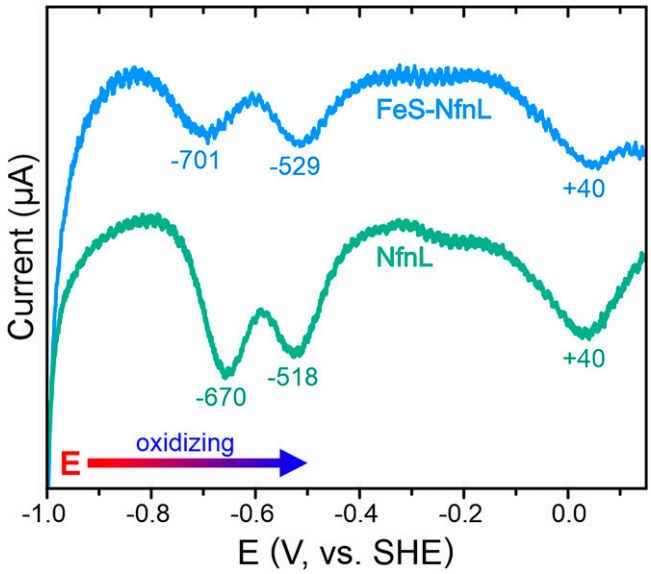

Fig. 3. SWV data of fully reconstituted NfnL (green) and FeS-NfnL (blue). NfnL showed peaks at −670 and −518 mV; FeS-NfnL displayed signals at −701 and −529 mV, which were assigned as the proximal and distal Fe/S clusters. The additional peak at +40 mV was present only in this direction and was assigned as the L-FAD $E_{m,ASQ/HQ}$.

energy gap of 279 mV. Direct measurement of the L-FAD $E_{m,ASQ/HQ}$, in conjunction with the $E_{m,Ox/HQ}$ couple, further minimizes any uncertainty associated with L-FAD $E_{m,Ox/ASQ}$.

Collectively, these values change our understanding of NfnSL interactions with the NADP(H) pool and how bifurcation is initiated within Nfn. The high affinity of NfnL for NADPH, along with the 1.8 Å distance from substrate to L-FAD (4), are sufficient to overcome the thermodynamic barrier for reduction of the bifurcating flavin by NADPH. Altogether, our measurements imply that the functional activity of NfnSL in vivo is likely constrained to a specific redox poise of the NADP(H) pool, given the negative $E_{m,Ox/HQ}$ of L-FAD. Therefore, the reduction potential of L-FAD defines not only the energy landscape of NfnSL but also the regime in which electron bifurcation operates within the cell.

The first bifurcated ET event in NfnSL (to the +80 mV [2Fe-2S]) is in fact thermodynamically favorable and the diminished energetic barrier now expedites this step by two orders of magnitude (Fig. 4). Previously, this process was understood to be uphill and kinetically slow, a feature that was hypothesized to ensure no accumulation of ASQ which could lead to unproductive reactions (36). However, the crossed potentials of L-FAD and the short-lived ASQ intermediate alleviate this possibility. The intricate tuning of cofactor reduction potential and proximity within the protein scaffold affords NfnSL the ability to reversibly bifurcate electrons with high efficiency. Indeed, a slight flattening of the first ET step along the high-potential branch may be necessary for the mechanism utilized during the reverse reaction (the formation of two NADPH resulting from the oxidation of two reduced Fd and one NADH, a process termed "confurcation") and is consistent with a nearly 1:1 activity ratio for bifurcation:confurcation in vitro.

Suppression of potential uncoupling pathways (termed "short-circuits") are crucial for productive catalysis (37–39). Although the rate for the short-circuit reaction in which L-FAD HQ reduces the proximal [4Fe-4S] (SC1, see Fig. 4) is increased by 10^4 s^{-1} from the previous model, the on-path ET event is still favored by just over three orders of magnitude

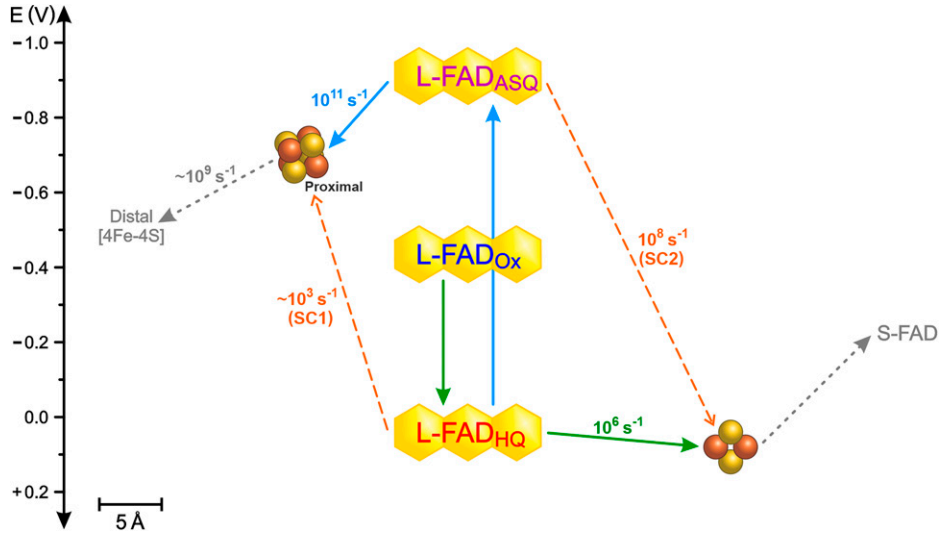

Fig. 4. Summary of the detailed energetic landscape of the NfnSL bifurcating flavin, L-FAD. Solid green and blue arrows represent empirically derived values for the high-potential and low-potential catalytic branches respectively, and long-dashed orange arrows depict two short-circuit pathways from the bifurcating flavin (SC1 and SC2). Cofactors, with the exception of S-FAD which was not assessed in this work, are scaled vertically based on reduction potentials and horizontally based on the shortest edge-to-edge distance between cofactors (4). Grayed cofactors and short-dashed arrows represent pathways not participating in direct electron transfer to or from the bifurcating flavin (4). Calculated k_{ET} values are shown alongside corresponding arrows.

(*SI Appendix*, Table S3). After the initial electron transfer, a short-circuit, where L-FAD ASQ reduces the [2Fe-2S] cluster (SC2), could be envisioned. However, due to the large separation in reduction potentials, this process lies in the Marcus inverted region with a rate constant that is inhibited by 10^3 s^{-1} compared to the productive catalytic route (*SI Appendix*, Table S3). This property arises from the steep free-energy slopes within the individual branches, a feature that is consistent with theoretical models of a universal free-energy landscape recently described for electron bifurcation (13). Despite flattening of the NfnSL energy landscape for the initial electron transfer for the first bifurcated electron, the steep thermodynamically uphill nature of the overall high-potential branch in NfnSL is preserved, as the terminal electron acceptor of this pathway, NAD^+, possesses a formal reduction potential of −320 mV. Further, the overall magnitude of the uphill electron transfer events across the high-potential branch (from bifurcating cofactor SQ/HQ to high-potential branch substrate) is comparable between our newly established NfnSL landscape and the quinone-based cytochrome bc_1 complex, at ∼+300 mV (8). Short-circuit reactions have been proposed to be influenced by the semiquinone stability constant, K_S (Eq. **4**) (9), whereby a sufficiently negative $\log K_S$ is indicative of inverted potentials and presumed to contribute to their prevention (9, 37, 38, 40, 41). A refined $\log K_S$ of −16.1 was determined for NfnSL L-FAD based on the results presented here, shifting it within range of other electron bifurcating systems (*SI Appendix*, Table S4), despite variability in bifurcating cofactor identities, reduction potentials, and overall energy landscapes (25, 26, 27, 42–46).

Interestingly, the bifurcation mechanism of NfnSL does not appear to require mass conformational movements (47) to specifically favor ET events, as seems to be the case for both quinone-based bifurcation (40, 48, 49) and the FBEB electron-transfer flavoproteins (Etf) (26, 50). Implementation of an initial uphill ET step, on the order of 200–300 mV, has been reported in these systems (25, 26, 27). When operating in these more positive potential ranges, a kinetically slow step may be necessary to coordinate the initiation of bifurcation with the large-scale conformational movements that occur after the first ET. NfnSL encompasses a sufficiently large energy gap, which is more negative relative to other bifurcating enzymes, allowing for increased plasticity to place unproductive ET events into disfavored regimes. Ultimately these differences enhance our understanding of the breadth of mechanisms that can be exploited to perform challenging, endergonic transformations. The subtle differences are expected to illuminate the more intricate phenomena involved in the control of bifurcated electrons, such as coupling of ET with proton transfer or alterations in flavin orientation and environment.

Elucidation of the bifurcating flavin reduction potentials in NfnSL underscores the richness of energetic landscapes employed by electron bifurcating systems and illuminates emerging features surrounding the stability of bifurcating cofactor intermediates. An accurate description of the energy transformation and coupling mechanisms employed by NfnSL is integral to the understanding of how energy is controlled and manipulated in complex biological systems; the insights of which will lead to design principles that accelerate the development of transformative energy technologies.

Materials and Methods

Steady-State Kinetics. Because NfnL alone cannot perform the electron bifurcation reaction carried out by NfnSL, due to the absence of the high-potential pathway housed in NfnS, decreased activity with NADPH as substrate was expected for the isolated large subunit. Further, the NADPH substrate-binding site is near the protein-protein interface between the small and large subunits, so it is also possible that isolated NfnL may exhibit an altered binding affinity for NADPH versus the native heterodimeric form of the enzyme. In order to quantitatively assess the activity in NfnL, dye-based steady-state kinetics experiments using 1 mM benzyl viologen were carried out with 1 mg × mL^{-1} enzyme (∼12 μM for NfnSL and ∼19 μM for NfnL) in buffer A at room temperature and under anoxic conditions. NADPH was added to NfnSL in a cuvette while stirring to concentrations ranging from 0.1 to 5.0 mM. Reduction of benzyl viologen by NfnSL was monitored by the increase in absorbance at 600 nm on OceanView software using an Ocean Optics HDX miniature spectrometer equipped with a 10-μm entrance slit, a CUV-ALL-UV cuvette holder, custom 200-μm diameter solarization-resistant fibers, and a DH-2000-BAL deuterium-tungsten halogen light source. A 25-ms spectral integration time was used with a boxcar width of 5 and each spectrum resulted from an average of 100 scans. The initial velocity

at this wavelength resulting from each concentration of NADPH was fit to a linear function. The slope of each fitted line was then graphed as a function of NADPH concentration and fit in OriginPro to a Michaelis-Menten function, described below by Eq. **2**, where V_{max} is the maximal velocity with saturating concentrations of substrate and K_M is the Michaelis-Menten constant. These experiments yielded K_M values for NADPH of 204 ± 11 μM in NfnSL (*SI Appendix*, Fig. S1*A*) and 1.16 ± 0.08 mM in NfnL (*SI Appendix*, Fig. S1*B*).

$$y = (V_{max}x)/(K_M + x). \quad [2]$$

Spectroelectrochemical (SEC) Studies. SEC experiments for measurement of the NfnL-FAD two-electron (oxidized-to-hydroquinone, or Ox/HQ) reduction potential were carried out in a 3D-printed cell housed in a quartz cuvette according to the specifications of Brisendine et al. (51), except at a volume of 500 μL. The cell consisted of a gold working electrode, platinum counter electrode, and a Microelectrodes MI-402 flexible Ag/AgCl/3 M KCl reference electrode. The reaction mixture included 15–20 μM reconstituted NfnL along with 1.5–2 μM each of phenosafranine, benzyl viologen, methyl viologen, and ethyl viologen in buffer A. Spectra were collected across a 200–800 nm wavelength range using the Ocean Optics apparatus described above and sampling every 30 s for 3–60 min for each potential applied. A CH Instruments 630C Potentiostat was used with CHI630C Software for amperometric current vs. time measurements with sampling intervals of 0.1 s and sensitivity of 1×10^{-4} A × V^{-1}. The solution was considered to be equilibrated once the absorbance at 450 nm remained stable following a minimization of current for each applied potential. Spectra were processed and analyzed using OriginPro software. Reduction of the NfnL-FAD was assessed using a decrease in absorbance at 450 nm, where interference from the two [4Fe-4S] clusters was minimal but the changes to the flavin could be well-visualized. Difference spectra for free FAD and NfnL L-FAD demonstrate that the signal change derives from flavin at 450 nm (*SI Appendix*, Fig. S8). The change in absorbance at this wavelength was graphed as a function of the applied potential and fit to a Nernst function, which revealed an Ox/HQ potential of −436 ± 8 mV with transfer of 2.0 ± 0.1 electrons. Values reported at pH 8.8 resulted from the average of four replicate measurements, three in the reducing direction and one in the oxidizing one. To be certain that the mediator dyes did not interfere with the measurement, one data set utilized only 0.75 μM benzyl viologen and methyl viologen (which do not have significant absorbance changes at 450 nm) and the absence of phenosafranine and ethyl viologen. Aside from requiring longer equilibration times during data collection, results from this data set were indistinguishable from those that included higher concentrations of all four dyes. An additional analysis was performed in the same buffer at pH 8.0 but showed no significant difference from the pH 8.8 data sets. The measured potentials using the Ag/AgCl/3 M KCl reference electrode were converted to the standard hydrogen electrode (SHE) values reported herein by the addition of 210 mV (52). The revised one-electron potentials for L-FAD, reported in *SI Appendix*, Table S2, were calculated according to Eq. **3** below, from the value reported here for the L-FAD two-electron couple along with the previously reported (4) Ox-to-semiquinone (Ox/SQ) couple for the L-FAD. Calculations of the flavin SQ stability constant (*SI Appendix*, Table S4), K_S, were carried out according to Eq. **4** below, where F is the Faraday constant (96,485 C × mol^{-1}), R is the ideal gas constant (8.314 J × mol^{-1} × K^{-1}), T is 298.15 K, and ΔE is the potential of the SQ/HQ couple subtracted from the Ox/SQ couple (9).

$$E_{Ox/HQ} = \frac{1}{2}E_{Ox/SQ} + \frac{1}{2}E_{SQ/HQ}, \quad [3]$$

$$\Delta E = \frac{2.3RT}{F}\log K_S. \quad [4]$$

Electrochemistry. Protein-film square-wave voltammetry (SWV) measurements were performed to assess the reduction potentials of the two [4Fe-4S] clusters housed within NfnL. A three-electrode 100 mL standard cell (Pine Research, RRPG021) apparatus comprised of a nonrotating, fixed disk pyrolytic graphite edge (PGE) working electrode (Pine Research, AFE1E0505GE), low profile Ag/AgCl/saturated KCl reference electrode (Pine Research, RRPEAGCL), and platinum wire counter electrode (BASi, MW-4130) was utilized for these experiments. The electrode was polished using an alumina slurry (BASi, CF-1050) and alumina polishing pads (BASi, MF-1040) and rinsed thoroughly prior to application of the protein film. NfnL was adsorbed to the electrode by application of 5 μL of 45 μM NfnL, incubation for at least 10 min, and subsequent washing with Buffer A (pH 7.0 or pH 8.8). Protein was reapplied in this manner following each measurement due to a loss of film at lower potentials. Experiments were carried out in a minimum of three replicates in an anaerobic chamber (Coy Laboratory Products), with Buffer A (at pH 7 or 8.8) in the standard cell while stirring at room temperature. Data were collected with potential (E) applied in both the oxidizing (i.e., negative-to-positive E; Fig. 3) and reducing (i.e., positive-to-negative E; *SI Appendix*, Fig. S5) directions with time in increments of 0.001 V at an amplitude of 0.025 V, a frequency of 10 Hz, and using a sensitivity setting of 1×10^{-6} A × V^{-1} with a CH Instruments 630C Potentiostat and CHI630C software. Data acquisition was performed by simultaneous sampling of both the current and potential at a rate of 1 MHz (10^6 s^{-1}) for each channel. Buffer background measurements were achieved by scans performed under the same conditions, but with omission of the protein film. All potential values are reported versus SHE following conversion from the Ag/AgCl/saturated KCl reference electrode by addition of 199 mV. The contribution of FAD to the overall signal between −400 and −600 mV in the reducing direction (*SI Appendix*, Table S1) was determined by analysis and comparison of the SWV peak heights in NfnL (fully reconstituted) versus FeS-NfnL (reconstituted with only Fe and S, but still retaining 0.35 equivalents of flavin). The thermodynamic and kinetic parameters (*SI Appendix*, Table S3) resulting from these measured potentials (along with the FAD E_m values in *SI Appendix*, Table S2) were calculated using Eqs. **5**–**7** below (4). The Moser-Dutton formula (Eq. **7**), with the electronic factor (Eq. **5**) and the nuclear factor (Eq. **6**) as terms contributing to it, was used to tabulate the electron transfer rate constant, k_{ET} in s^{-1}, where $\Delta G°$ is the free energy in eV, R is the edge-to-edge distance between electron acceptor and donor in Å, β is a correction to the distance parameter that is proportional to barrier height equal to 1.1 $Å^{-1}$, γ is a nuclear term parameter equal to 3.1, and λ represents the reorganization energy of 0.7 eV (53).

$$\text{Electronic Factor} = (\beta(R - 3.6))/2.303, \quad [5]$$

$$\text{Nuclear Factor} = \gamma\left((\Delta G° + \lambda)^2/\lambda\right), \quad [6]$$

$$\log k_{ET} = 13 - ((\beta(R - 3.6))/2.303) - \left(\gamma\left((\Delta G° + \lambda)^2/\lambda\right)\right). \quad [7]$$

Equilibrium Fluorescence Binding Titrations. Fluorescence spectroscopy was used to quantitatively assess the interaction of NfnL with the NADPH and $NADP^+$ substrates. Data were collected via right-angle detection on a Horiba Fluorolog-3 fluorimeter from Jobin Yvon, Inc. equipped with FluorEssence software. NADPH and $NADP^+$ stocks were quantified spectroscopically prior to reaction set-up using the Beer-Lambert law with $\varepsilon_{340\ nm} = 6.22\ mM^{-1} \times cm^{-1}$ and $\varepsilon_{260\ nm} = 17.5\ mM^{-1} \times cm^{-1}$ for the reduced and oxidized pyridine nucleotides respectively. Samples consisting of 100 μL of 25 μM enzyme in buffer A were prepared anaerobically in a septum-sealed 3 × 3 mm fluorescence ultramicro cuvette (Hellma) and titrated with NADP(H) to final concentrations ranging from 5 to 100 μM. Following incubation at room temperature for at least 45 min to ensure complete equilibration of the binding reaction, the Trp and Tyr residues of NfnL were excited at 285 nm and emission spectra was collected from 300 nm to 500 nm in 1-nm increments with 5-nm excitation and emission slit widths. The decrease in fluorescence intensity at 345 nm, resulting from the quenched emission of Trp and Tyr residues in response to interaction of NfnL with the NADPH substrate, was graphed against NADPH concentration following correction for inner filter effects (54) and fit to a Morrison (quadratic) function (Eq. **8**) (55) using OriginPro. In this equation, K_D is the equilibrium binding dissociation constant, [E] denotes the total enzyme concentration, [S] is the total substrate concentration, and [ES] represents the concentration of enzyme bound to substrate. Thus, the ratio of [ES] to [E] yields the fraction of total enzyme that is bound to substrate, which is equal to the ratio of the change-in-fluorescence (ΔF) to the fitted maximal change-in-fluorescence (ΔF_{max}). Experiments with NADPH and $NADP^+$ were each performed in duplicate. NfnL affinity for the oxidized versus reduced forms of this substrate were largely identical and yielded a K_D value for NADP(H) of 3.0 ± 0.4 μM (*SI Appendix*, Fig. S4).

$$[ES]/[E] = \Delta F/\Delta F_{max} = \left((K_D + [E] + [S]) - \sqrt{(K_D + [E] + [S])^2 - (4[E][S])}\right)/(2[E]). \quad [8]$$

Data Availability. All study data are included in the article and/or *SI Appendix*.

ACKNOWLEDGMENTS. This work was authored in part by Alliance for Sustainable Energy, LLC, the manager and operator of the National Renewable Energy Laboratory for the US Department of Energy (DOE) under Contract No. DE-AC36-08GO28308. Funding was provided to C.E.W., A.E.L., D.W.M., K.J.C., P.W.K., and C.E.L. by the US DOE Office of Basic Energy Sciences (BES), Division of Chemical Sciences, Geosciences, and Biosciences. The DOE BES Physical Biosciences Program supported the generation of the enzyme expression system and constructs. Electrochemical, kinetic, and spectroscopic investigations were supported by the DOE Office of Science Early Career Program. The views expressed in the article do not necessarily represent the views of the DOE or the US government. The US government and the publisher, by accepting the article for publication, acknowledges that the US government retains a nonexclusive, paid-up, irrevocable, worldwide license to publish or reproduce the published form of this work, or allow others to do so, for US government purposes. J.W.P. was supported by the US DOE, Office of Science, Office of BES under Award DE-FG02x04ER15563. Partial salary support for J.W.P. was funded by the US Department of Agriculture National Institute of Food and Agriculture (Hatch umbrella project 1015621).

1. W. Buckel, R. K. Thauer, Energy conservation via electron bifurcating ferredoxin reduction and proton/Na(+) translocating ferredoxin oxidation. *Biochim. Biophys. Acta* **1827**, 94–113 (2013).
2. F. Li *et al.*, Coupled ferredoxin and crotonyl coenzyme A (CoA) reduction with NADH catalyzed by the butyryl-CoA dehydrogenase/Etf complex from *Clostridium kluyveri*. *J. Bacteriol.* **190**, 843–850 (2008).
3. J. W. Peters, A. F. Miller, A. K. Jones, P. W. King, M. W. Adams, Electron bifurcation. *Curr. Opin. Chem. Biol.* **31**, 146–152 (2016).
4. C. E. Lubner *et al.*, Mechanistic insights into energy conservation by flavin-based electron bifurcation. *Nat. Chem. Biol.* **13**, 655–659 (2017).
5. P. Mitchell, The protonmotive Q cycle: A general formulation. *FEBS Lett.* **59**, 137–139 (1975).
6. U. Brandt, Energy conservation by bifurcated electron-transfer in the cytochrome-bc1 complex. *Biochim. Biophys. Acta* **1275**, 41–46 (1996).
7. K. Kayastha, S. Vitt, W. Buckel, U. Ermler, Flavins in the electron bifurcation process. *Arch. Biochem. Biophys.* **701**, 108796 (2021).
8. C. E. Wise, A. E. Ledinina, J. L. Yuly, J. H. Artz, C. E. Lubner, The role of thermodynamic features on the functional activity of electron bifurcating enzymes. *Biochim. Biophys. Acta Bioenerg.* **1862**, 148377 (2021).
9. F. Baymann *et al.*, On the natural history of flavin-based electron bifurcation. *Front. Microbiol.* **9**, 1357 (2018).
10. J. W. Peters, D. N. Beratan, G. J. Schut, M. W. W. Adams, On the nature of organic and inorganic centers that bifurcate electrons, coupling exergonic and endergonic oxidation-reduction reactions. *Chem. Commun. (Camb.)* **54**, 4091–4099 (2018).
11. W. Buckel, R. K. Thauer, Flavin-based electron bifurcation, ferredoxin, flavodoxin, and anaerobic respiration with protons (Ech) or NAD^+ (Rnf) as electron acceptors: A historical review. *Front. Microbiol.* **9**, 401 (2018).
12. J. W. Peters *et al.*, A new era for electron bifurcation. *Curr. Opin. Chem. Biol.* **47**, 32–38 (2018).
13. J. L. Yuly, P. Zhang, C. E. Lubner, J. W. Peters, D. N. Beratan, Universal free-energy landscape produces efficient and reversible electron bifurcation. *Proc. Natl. Acad. Sci. U.S.A.* **117**, 21045–21051 (2020).
14. A. F. Miller, H. D. Duan, T. A. Varner, N. Mohamed Raseek, Reduction midpoint potentials of bifurcating electron transfer flavoproteins. *Methods Enzymol.* **620**, 365–398 (2019).
15. V. Müller, Energy conservation in acetogenic bacteria. *Appl. Environ. Microbiol.* **69**, 6345–6353 (2003).
16. F. L. Sousa, M. Preiner, W. F. Martin, Native metals, electron bifurcation, and CO_2 reduction in early biochemical evolution. *Curr. Opin. Microbiol.* **43**, 77–83 (2018).
17. Z. Yan, J. G. Ferry, Electron bifurcation and confurcation in methanogenesis and reverse methanogenesis. *Front. Microbiol.* **9**, 1322 (2018).
18. S. Wang, H. Huang, J. Moll, R. K. Thauer, $NADP^+$ reduction with reduced ferredoxin and $NADP^+$ reduction with NADH are coupled via an electron-bifurcating enzyme complex in *Clostridium kluyveri*. *J. Bacteriol.* **192**, 5115–5123 (2010).
19. B. Schoepp-Cothenet *et al.*, On the universal core of bioenergetics. *Biochim. Biophys. Acta* **1827**, 79–93 (2013).
20. W. Nitschke, M. J. Russell, Redox bifurcations: Mechanisms and importance to life now, and at its origin: A widespread means of energy conversion in biology unfolds … . *BioEssays* **34**, 106–109 (2012).
21. D. H. Evans, One-electron and two-electron transfers in electrochemistry and homogeneous solution reactions. *Chem. Rev.* **108**, 2113–2144 (2008).
22. P. S. Brereton, M. F. Verhagen, Z. H. Zhou, M. W. Adams, Effect of iron-sulfur cluster environment in modulating the thermodynamic properties and biological function of ferredoxin from *Pyrococcus furiosus*. *Biochemistry* **37**, 7351–7362 (1998).
23. W. R. Hagen *et al.*, Novel structure and redox chemistry of the prosthetic groups of the iron-sulfur flavoprotein sulfide dehydrogenase from *Pyrococcus furiosus*; evidence for a [2Fe-2S] cluster with Asp(Cys)3 ligands. *J. Biol. Inorg. Chem.* **5**, 527–534 (2000).
24. W. Buckel, R. K. Thauer, Flavin-based electron bifurcation, a new mechanism of biological energy coupling. *Chem. Rev.* **118**, 3862–3886 (2018).
25. G. J. Schut *et al.*, The catalytic mechanism of electron-bifurcating electron transfer flavoproteins (ETFs) involves an intermediary complex with NAD^+. *J. Biol. Chem.* **294**, 3271–3283 (2019). Correction in: *J. Biol. Chem.* **295**, 15423 (2020).
26. J. K. Demmer, N. Pal Chowdhury, T. Selmer, U. Ermler, W. Buckel, The semiquinone swing in the bifurcating electron transferring flavoprotein/butyryl-CoA dehydrogenase complex from *Clostridium* difficile. *Nat. Commun.* **8**, 1577 (2017).
27. J. Sucharitakul *et al.*, Modulations of the reduction potentials of flavin-based electron bifurcation complexes and semiquinone stabilities are key to control directional electron flow. *FEBS J.* **288**, 1008–1026 (2021).
28. F. L. Rodkey, J. A. Donovan Jr., Oxidation-reduction potentials of the triphosphopyridine nucleotide system. *J. Biol. Chem.* **234**, 677–680 (1959).
29. S. K. Spaans, R. A. Weusthuis, J. van der Oost, S. W. Kengen, NADPH-generating systems in bacteria and archaea. *Front. Microbiol.* **6**, 742 (2015).
30. W. Nernst, *Experimental and Theoretical Applications of Thermodynamics to Chemistry* (Charles Scribner's Sons, New York, NY, 1907).
31. W. Curtis *et al.*, "Mitigation of damage from reactive oxygen species and ionizing radiation by ketone body esters" in *Ketogenic Diet and Metabolic Therapies: Expanded Roles in Health and Disease*, S. A. Masino, Ed. (Oxford University Press, New York, NY, 2017), chap. 27, pp. 254–270.
32. H. A. Krebs, R. L. Veech, "Pyridine nucleotide interrelations" in *The Energy Level and Metabolic Control in Mitochondria*, S. Papa, J. M. Tager, E. Quagliariello, E. C. Slator, Eds. (Adriatica Editrice, Bari, Italy, 1969), pp. 329–384.
33. W. Xiao, R. S. Wang, D. E. Handy, J. Loscalzo, NAD(H) and NADP(H) redox couples and cellular energy metabolism. *Antioxid. Redox Signal.* **28**, 251–272 (2018).
34. F. Q. Schafer, G. R. Buettner, Redox environment of the cell as viewed through the redox state of the glutathione disulfide/glutathione couple. *Free Radic. Biol. Med.* **30**, 1191–1212 (2001).
35. M. Lovrić, Š. Komorsky-Lovrić, Theory of square-wave voltammetry of two-electron reduction with the adsorption of intermediate. *Int. J. Electrochem.* **2012**, 596268 (2012).
36. P. Zhang *et al.*, Electron bifurcation: Thermodynamics and kinetics of two-electron brokering in biological redox chemistry. *Acc. Chem. Res.* **50**, 2410–2417 (2017).
37. A. Osyczka, C. C. Moser, P. L. Dutton, Fixing the Q cycle. *Trends Biochem. Sci.* **30**, 176–182 (2005).
38. L. Bergdoll, F. Ten Brink, W. Nitschke, D. Picot, F. Baymann, From low- to high-potential bioenergetic chains: Thermodynamic constraints of Q-cycle function. *Biochim. Biophys. Acta* **1857**, 1569–1579 (2016).
39. J. L. Yuly, C. E. Lubner, P. Zhang, D. N. Beratan, J. W. Peters, Electron bifurcation: Progress and grand challenges. *Chem. Commun. (Camb.)* **55**, 11823–11832 (2019).
40. A. Osyczka, C. C. Moser, F. Daldal, P. L. Dutton, Reversible redox energy coupling in electron transfer chains. *Nature* **427**, 607–612 (2004).
41. S. Jünemann, P. Heathcote, P. R. Rich, On the mechanism of quinol oxidation in the bc1 complex. *J. Biol. Chem.* **273**, 21603–21607 (1998).
42. H. Zhang, A. Osyczka, P. L. Dutton, C. C. Moser, Exposing the complex III Qo semiquinone radical. *Biochim. Biophys. Acta* **1767**, 883–887 (2007).
43. H. Zhang *et al.*, Quinone and non-quinone redox couples in Complex III. *J. Bioenerg. Biomembr.* **40**, 493–499 (2008).
44. H. Ding *et al.*, Ubiquinone pair in the Qo site central to the primary energy conversion reactions of cytochrome bc1 complex. *Biochemistry* **34**, 15979–15996 (1995).
45. A. R. Crofts *et al.*, The mechanism of ubihydroquinone oxidation at the Qo-site of the cytochrome bc1 complex. *Biochim. Biophys. Acta* **1827**, 1362–1377 (2013).
46. N. P. Chowdhury, K. Klomann, A. Seubert, W. Buckel, Reduction of flavodoxin by electron bifurcation and sodium ion-dependent reoxidation by NAD^+ catalyzed by ferredoxin-NAD^+ reductase (Rnf). *J. Biol. Chem.* **291**, 11993–12002 (2016).
47. L. Berry *et al.*, H/D exchange mass spectrometry and statistical coupling analysis reveal a role for allostery in a ferredoxin-dependent bifurcating transhydrogenase catalytic cycle. *Biochim. Biophys. Acta, Gen. Subj.* **1862**, 9–17 (2018).
48. A. R. Crofts, The Q-cycle – A personal perspective. *Photosynth. Res.* **80**, 223–243 (2004).
49. A. R. Crofts *et al.*, The Q-cycle mechanism of the bc_1 complex: A biologist's perspective on atomistic studies. *J. Phys. Chem. B* **121**, 3701–3717 (2017).
50. J. K. Demmer *et al.*, Molecular basis of the flavin-based electron-bifurcating caffeyl-CoA reductase reaction. *FEBS Lett.* **592**, 332–342 (2018).
51. J. M. Brisendine, A. C. Mutter, J. F. Cerda, R. L. Koder, A three-dimensional printed cell for rapid, low-volume spectroelectrochemistry. *Anal. Biochem.* **439**, 1–3 (2013).
52. E. P. Friis *et al.*, Metalloprotein adsorption on Au(111) and polycrystalline platinum investigated by in situ scanning tunneling microscopy with molecular and submolecular resolution. *Electrochim. Acta* **43**, 2889–2897 (1998).
53. C. C. Page, C. C. Moser, X. Chen, P. L. Dutton, Natural engineering principles of electron tunnelling in biological oxidation-reduction. *Nature* **402**, 47–52 (1999).
54. M. O. Palmier, S. R. Van Doren, Rapid determination of enzyme kinetics from fluorescence: Overcoming the inner filter effect. *Anal. Biochem.* **371**, 43–51 (2007).
55. J. F. Morrison, Kinetics of the reversible inhibition of enzyme-catalysed reactions by tight-binding inhibitors. *Biochim. Biophys. Acta* **185**, 269–286 (1969).